High-Spatial Resolution Giant Magnetoresistive Sensors – Part I: Application in Non-Destructive Evaluation

K. Chomsuwan[1], T. Somsak[2], C.P. Gooneratne[3], and S. Yamada[4]

[1] King Mongkut's University of Technology Thonburi, Bangkok, Thailand
[2] Rajamangala University of Technology Lanna, Chiang-Mai, Thailand
[3] King Abdullah University of Science and Technology, Thuwal, Saudi Arabia
Chinthaka.Gooneratne@kaust.edu.sa
[4] Kanazawa University, Kanazawa, Japan

Abstract. In this chapter, we report the utilization of spin-valve type giant magnetoresistance (GMR) sensors in non-destructive evaluation (NDE). The NDE application is the inspection of high-density printed circuit boards (PCBs) based on the eddy-current testing (ECT) technique. An ECT probe with a GMR sensor is presented for the inspection of high-density double-layer PCB models. The utilization of a GMR sensor as a magnetic sensor showed that PCB inspection could be performed with high-spatial resolution and sensitivity, over a large frequency range.

1 Introduction

Giant magnetoresistance (GMR) sensors have great potential to be used as magnetic field detectors because they are sensitive to low-magnetic fields with high spatial resolution and can be easily integrated with existing semiconductor electronics [1-13]. Due to advancements in micro/nano technology they can be expanded to compact array structures and fabricated in a large scale [14-18]. GMR sensors are energized by applying a constant current and the output voltage is an indication of the change in resistance due to the change in applied magnetic field. High spatial resolution GMR probes are presented in this chapter for inspection of printed circuit boards (PCBs).

Electrical contact tests, and/or non-electrical, non-contact methods such as automatic visual/optical inspection, have been routinely used for the inspection of PCBs for defects for many years [19-25]. While electrical tests can be used to obtain information about many types of defects it cannot detect potential defects such as line width or spacing reductions. Automatic visual/optical inspection procedures are inexpensive and provides high throughput but can only inspect the outer surface of a PCB. Eddy-current testing (ECT) is a popular non-contact, non-destructive evaluation (NDE) method that is usually applied to evaluate material flaws without changing or altering the material under test [26, 27]. Defects on a PCB conductor can be

C. Reig et al.: *Giant Magnetoresistance (GMR) Sensors*, SSMI 6, pp. 211–241.
DOI: 10.1007/978-3-642-37172-1_9

investigated by eddy-current flow. The ECT probe employed in this research for the inspection of PCBs consists of a planar meander coil for excitation and a GMR sensor for detection. The aims of this research is to use the ECT probe to analyze and enhance the ECT signal for the easy identification of any defect points on the PCB conductor, to improve the scanning speed and resolution for detecting imperfections of the PCB conductor, and also to obtain PCB conductor dimensions and alignment.

2 ECT Technique Based Application

2.1 Introduction

NDE is an examination, test, or evaluation performed on any type of tested object without changing or altering that object in any way, in order to determine the absence or presence of conditions or discontinuities that may have an effect on the usefulness or serviceability of that object [28, 29]. NDE may also be conducted to measure other test object characteristics, such as size; dimension; configuration; or structure, including alloy content, hardness, grain size, etc. The most common NDE methods are visual inspection, magnetic particle testing and ultrasonic testing. ECT is an NDE technique which is sensitive to very small cracks or flaws on a test specimen surface and subsurface. Several high-performance ECT probes have been developed based on exciting coils and magnetic sensors for, detecting dangerous cracks around fastener hole and engine components in aircrafts [30-33], and inspection of cracks, flaws as well as corrosion in power plant equipment, reactor, turbine, thick structures and pipeline systems [34-37]. Magnetic sensors play a key role in ECT-based inspection systems [38]. Several kinds of magnetic sensors such as Hall, GMR, SQUID, etc. have been successfully used as ECT probes for non-destructive detection of material cracks [39]. Moreover, inspection techniques such as multi frequency ECT and pulse ECT have been developed for thin metal tubes and sheets, as well as metal cladding for measuring thickness and for the location and sizing of internal defects [40].

Eddy-currents are closed loops of induced current circulating in a plane perpendicular to the direction of a time varying magnetic flux density $\boldsymbol{B}$. The variation of $\boldsymbol{B}$, generates an electric field intensity $\boldsymbol{E}$, in the loop as expressed by Maxwell's equation in equation (1).

$$\nabla \times \boldsymbol{E} = -\frac{\partial \boldsymbol{B}}{\partial t}. \tag{1}$$

Therefore, the current density $\boldsymbol{J}$, in a material with conductivity σ, also circulates in the loop because:

$$\boldsymbol{J} = \sigma \boldsymbol{E}, \tag{2}$$

where $\boldsymbol{B}$, $\boldsymbol{E}$, $\boldsymbol{J}$ and σ are in T, V/m, A, and S/m respectively.

Eddy-currents are referred to as "eddy-current losses" when they occur in electrical machines such as motors and transformers because they degrade the performance of such devices. On the contrary, eddy-currents are useful when applied to detect flaws or cracks on metallic materials; this forms the basis for the ECT technique.

The frequency of the applied magnetic flux has an effect on how deep the electric field intensity penetrates into the conductive material. Its amplitude is attenuated exponentially with depth. The distance through which the amplitude decreases by a factor e^{-1} is known as the "skin depth" or the "penetration depth" of the material and it can be expressed as

$$\delta = \frac{1}{\sqrt{\pi f \mu \sigma}}, \tag{3}$$

where δ is the skin depth (m), f is the frequency of B (Hz) and μ is the permeability.

Skin effect arises when the eddy-currents flowing in the test object at any depth produce a magnetic flux which opposes the primary flux, thus reducing the total magnetic flux and causing a decrease in current flow as depth increases. Alternatively, eddy-currents near the surface can be viewed as shielding the coil's magnetic flux, thereby weakening the magnetic flux at greater depths and reducing induced currents. From equation (3), increasing of frequency of the applied B, σ and μ of the specimen are the cause of decreasing of skin depth. This effect is very useful when it is applied to ECT technique for detection of cracks or flaws on conductive material at difference depths.

The proposed ECT probe consists of an exciting coil and a magnetic sensor as shown in Fig. 1. A sinusoidal current is fed to the exciting coil to generate a B over the conductive material. Eddy-currents are induced and circulate in the conductive material due to the B from the exciting coil; the eddy-currents in turn also generate its own B. B generated from eddy-currents are normally uniform. Therefore, the output signal that is obtained from the pick-up coil is constant. Whenever there is a defect on the conductive material, eddy-currents change its path leading to a non-uniform B, resulting in a change in the output signal at the pick-up coil; thus defect points can be identified on a given material under test.

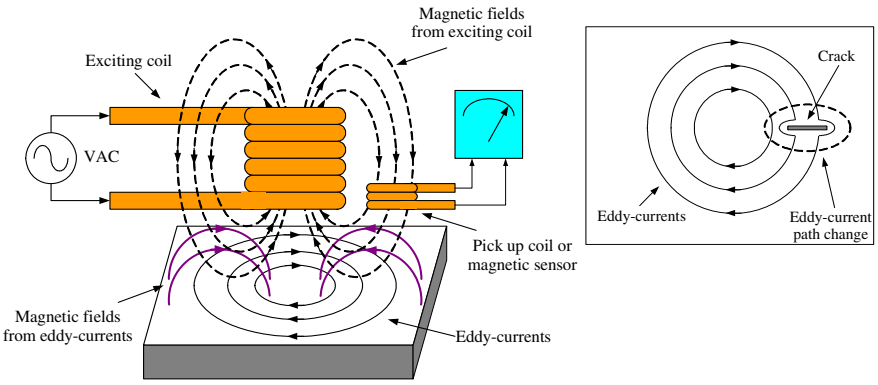

Fig. 1. Basic principle of eddy-current testing technique on crack detection

Eddy-currents can be applied to test not only cracks or flaws but also the following variables:

- Conductivity variations
- Spacing between probe and specimen
- Material thickness
- Thickness of plating or cladding on a base material
- Spacing between conductive layers
- Permeability variations

Although the ECT technique can be used for many applications, many factors such as conductivity, permeability, lift-off height and coil design have an influence on test performance.

2.2 PCB Inspection Based on ECT Technique

2.2.1 Design and Construction of the ECT Probe

The proposed ECT probe, which consists of a long planar meander coil serving as an exciting coil, and a magnetic sensor, was fabricated for PCB inspection as shown in Fig. 2. The long planar meander coil was used as an exciting coil because it provides the advantages of easily developing the matrix sensor to improve the scanning speed [41, 42] and of providing a short distance between the sensor and tested object. The long planar meander coil was made from copper with 35 µm thickness. Two films made from Polyimide are needed to separate the planar meander coil from the magnetic sensor and the PCB conductor. Thickness of the film is 50 µm therefore; the total thickness of the planar meander coil is around 135 µm. The two-dimensional (2-D) B distribution of the planar meander coil is shown in Fig. 3. This figure shows that the B generated by the planar meander coil are distributed only in the x and y direction.

Magnetic sensors have to be set up in the sensing direction in order to detect the B only in the scanning direction. As shown in Fig. 4, the spin-valve type GMR used as the magnetic sensor consists of 4 strips and each strip has dimensions of 100 µm × 18 µm. Therefore, the total effective area of the GMR sensor is 100 µm × 93 µm with a 7 µm gap between the strips. In comparison of sensor structure, it can be said that distance between the GMR sensor surface and PCB conductor or lift-off height is at least 135 µm, whereas other sensors such as solenoid coils have higher lift-off than the GMR sensor.

2.2.2 PCB Defect Detection Using the ECT Probe

High-frequency exciting currents are fed into the planar meander coil to generate a B distributed over the PCB conductor as shown in Fig. 5. The exciting currents normally

flow in z axis or scanning direction. The eddy-currents flowing in the PCB conductor are induced by the applied B and also flow in z axis or scanning direction. Because of the skin depth effect, the eddy-currents flow very close to surface or boundary of the PCB conductor. Whenever a defect or the PCB conductor boundary that is perpendicular to scanning direction is found, the eddy-currents will change its path and flow in x direction generating a magnetic flux density B_z, flowing in the z direction. Therefore, defects on the PCB conductor or the conductor boundary can be identified if B_z is detected. Partial defects, occurring on both PCB conductor width and PCB conductor thickness, also have an effect on the eddy-current path. As show in Fig. 6, low eddy-currents flowing in the x axis generate a weak B_z.

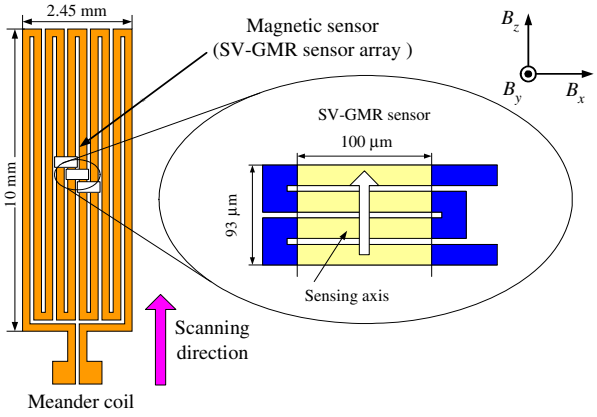

(a) Top view

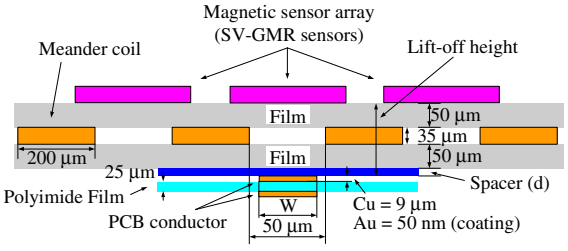

(b) Cross section

Fig. 2. Proposed ECT probe for printed circuit board inspection

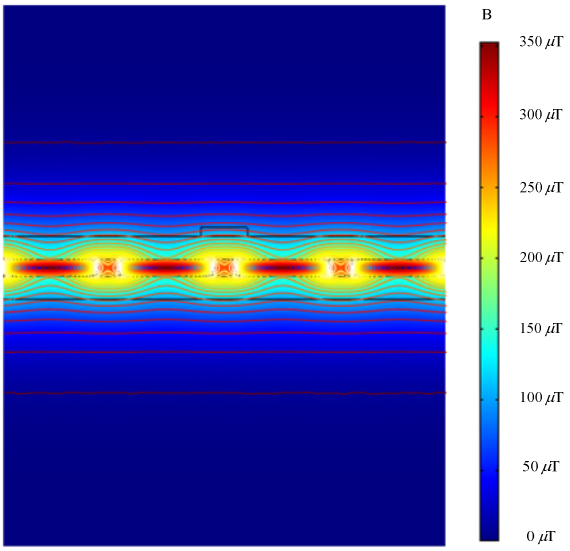

Fig. 3. Magnetic flux distribution obtained from a meander coil with 4 turns

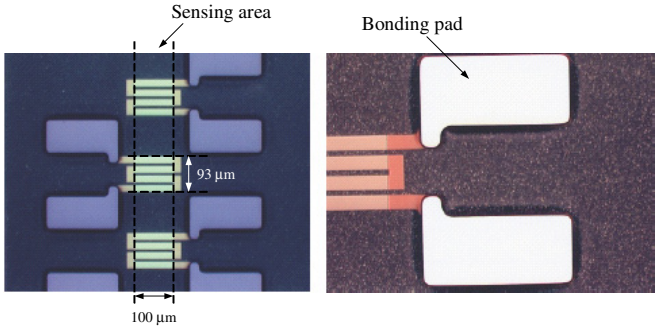

Fig. 4. The GMR sensors used in experiments

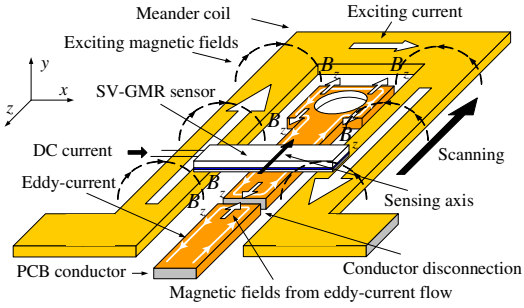

Fig. 5. Basic principle of ECT technique for printed circuit board inspection

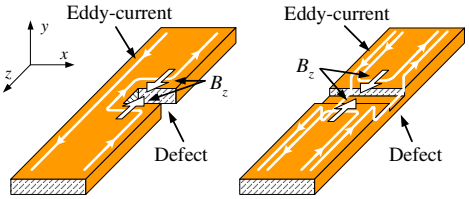

Fig. 6. Eddy-current paths for partial defects occurring on a PCB conductor, in width (left) and thickness (right)

It is more difficult to measure B_z than B_y, because B_z appears at a very short distance from the test PCB conductor and its value is not as high as B_y. However, B_z only appears when there are defects or at the boundaries of a PCB conductor. The output signal does not have to be extracted from other signals as in case of the inspection utilizing B_y. The magnetic sensor moving above the test PCB conductor is not penetrated by B_z until it encounters a defect; therefore, the magnetic sensor is less susceptible to noise in the output signal. This is a big advantage of the proposed ECT probe and the main reason for its high sensitivity. To detect the defect occurring on the PCB conductor, the magnetic sensor, therefore, has to detect only B_z or the magnetic flux density that is parallel to the scanning direction.

2.2.3 Finite Element Analysis of Eddy-Current Flow

Eddy-currents flowing in the PCB conductor and B distribution generated by the eddy-currents were studied based on the Finite Element Method (FEM). Three types of defects on the PCB conductor, namely conductor disconnections, partial defects on

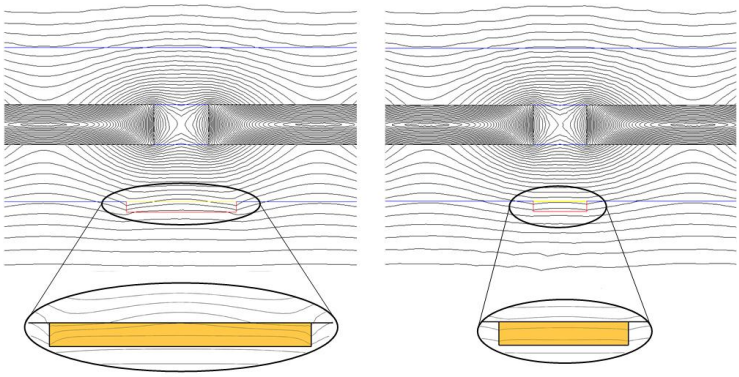

(a) 100 µm PCB conductor width. 50 µm PCB conductor width.

Fig. 7. Magnetic flux distribution over a PCB conductor at an exciting frequency of 5 MHz

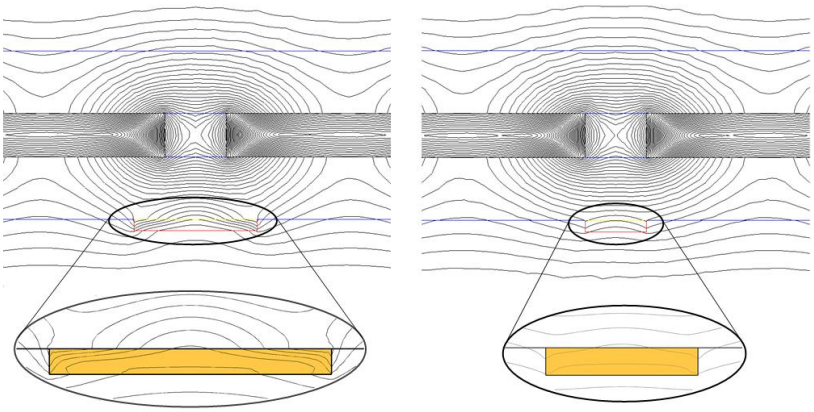

(a) 100 µm PCB conductor width. (b) 50 µm PCB conductor width.

Fig. 8. Magnetic flux distribution over a PCB conductor at an exciting frequency of 10 MHz

PCB conductor width, and partial defects on PCB conductor thickness, are analyzed. Disconnection length of 50 µm is allocated on the conductor disconnection model. For partial defects, the disconnection region also is set to 50 µm where the disconnection region is only 50 % of the PCB conductor. The skin depth or depth of penetration is an important parameter that must be considered. The skin depth of copper at a frequency of 5 MHz can be calculated by referring to equation (3). Sinusoidal current of 200 mA at a frequency of 5 MHz and 10 MHz was fed to the planar meander coil model to generate a B over the PCB conductor. As shown in Fig. 7, because of flux penetration effects, B distribution over the PCB conductor at a frequency of 5 MHz differs from one without a PCB conductor, as was seen in Fig. 3. A narrow PCB conductor has less effect than a wide PCB conductor. In case of high frequency (10 MHz) excitation, the flux penetration effect is stronger than that at a frequency of 5 MHz as shown in Fig. 8. Eddy-currents flow on a PCB conductor and the resulting magnetic flux distribution over the PCB conductor when a defect is found on the PCB conductor are shown in Fig. 9. Eddy-currents usually flow along the scanning direction, but whenever there is a defect or soldering point on the PCB conductor the eddy-currents change its path resulting in a measurable B_z. Moreover, the distribution of eddy-currents is mainly along the PCB conductor boundary because of skin depth effect. Therefore, peak values of B_z appear at the defect point region or the PCB conductor boundaries.

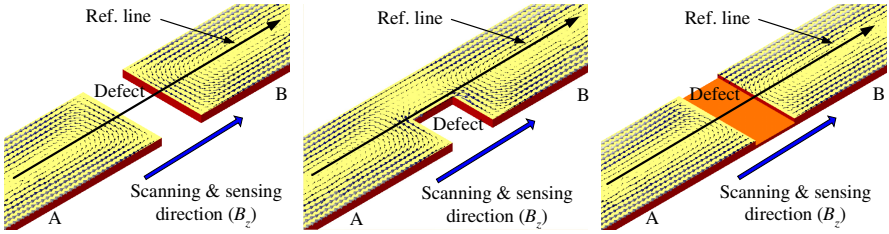

(a) Conductor disconnection. (b) Partial defect on track width. (c) Partial defect on thickness.

Fig. 9. Eddy-current flow in a PCB conductor for different types of defects

Based on FEM analysis, the magnetic flux distribution over a PCB conductor with defects is shown in Fig. 10. B_z fluctuates at the defect point or displacement distance at 0 mm. The wider PCB conductor generates a higher B_z variation than the narrow PCB conductor because of high-density eddy-current flow. For a partial defect on the PCB conductor track width, magnitude of magnetic flux density variation at partial defect on PCB track width does not differ from that of a conductor disconnection point. In addition, the effect of exciting frequency and PCB conductor width influences the B variation at a defect point. A partial defect on PCB thickness generates the lowest B variation because of low eddy-current flow. However, the B variation is high enough to be detected by the magnetic sensor.

2.2.4 Solder Microbead Detection by the ECT Probe

The proposed ECT probe is also applied to detect solder microbeads that are placed on the PCB for assembly; Ball Grid Array (BGA) package based on surface mounting technology. As shown in Fig. 11, the principle of solder microbead detection is similar to the inspection of PCB defects. Eddy-currents are induced by alternating exciting B which flow on the surface of the microbead. These eddy-currents generate a B_z that usually occur at the microbead boundary. Therefore, the ECT probe can obtain information about the position of the microbead by detecting B_z as in the case of PCB defect detection.

The same technique as mentioned above was applied to analyse the magnetic flux distribution obtained from eddy-current flow inside a solder microbead. The microbead size of 125 µm radius (250 µm diameter) was used in the analysis model. Eddy-currents are induced and flow in the microbead as shown in Fig. 12 and this eddy-current flow generates a B_z as shown in Fig. 13. The shape of the signal obtained in the solder ball region is very similar to the signal obtained at the disconnection point of the PCB conductor. At the microbead center, the signal changes from positive to negative at a displacement distance of 0 mm. Therefore, the FEM analysis results confirm that the proposed ECT probe can also be applied for the detection of solder microbeads.

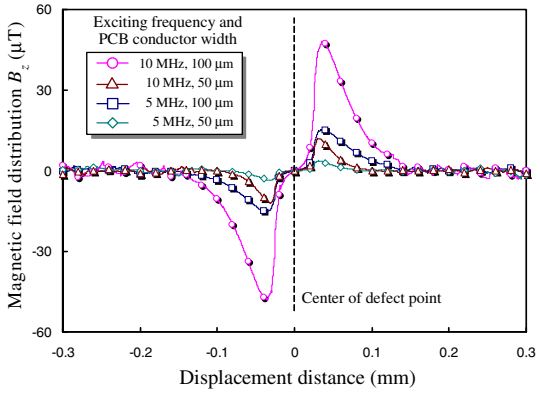

(a) Conductor disconnection

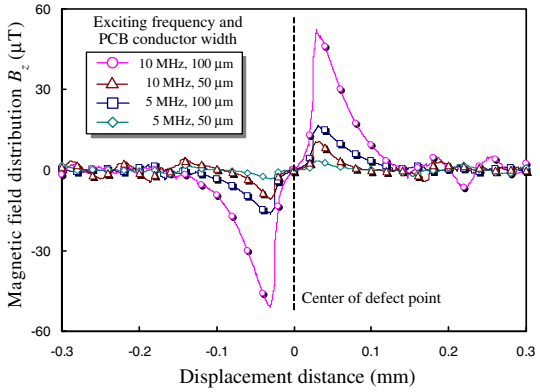

(b) Partial defect on track width

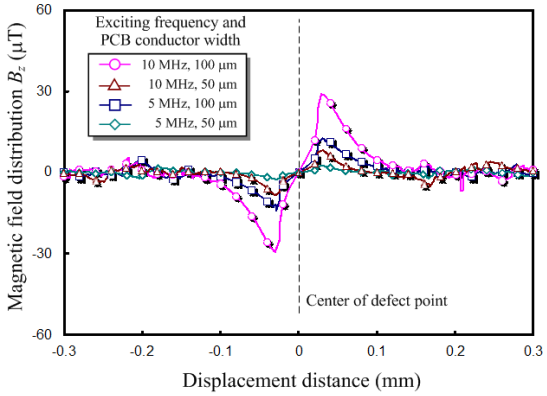

(c) Partial defect on thickness

Fig. 10. Magnetic flux density in scanning direction (B_z) for different defect types over the reference line, as in Fig. 9

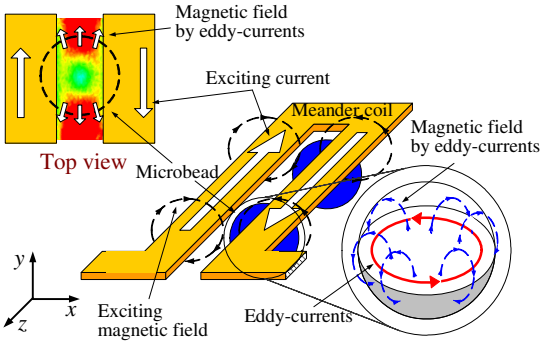

Fig. 11. Detection of solder microbeads by the ECT probe

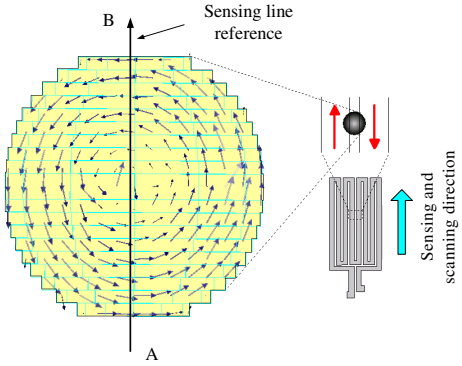

Fig. 12. Eddy-current flow inside a solder microbead of 125 µm radius when placed under a meander coil generating a magnetic flux density at a frequency of 5 MHz

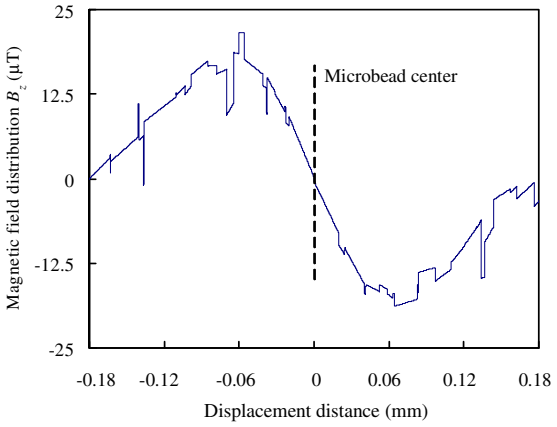

Fig. 13. Magnetic flux distribution B_z over the solder microbead obtained from FEM analysis; exciting frequency is 5 MHz

2.3 ECT Probe Characteristics and Inspection System

2.3.1 Characteristics of the GMR Sensor

A magnetic flux density ranging from -4 to 4 mT are generated by a DC exciting current that is fed to the Helmholtz coil. The nominal resistance of the GMR sensor is 400 Ω. The DC characteristic of the GMR sensor in its sensing axis is shown in Fig. 14. From the characteristics, the proposed GMR sensor has a maximum magnetoresistance ratio of approximately 12 % of its normal resistance, or has a resistance variation between 370 and 420 Ω. The linear region sensitivity of the proposed GMR is approximately 12 %/mT or 48 Ω/mT with a low hysteresis loop. Moreover, the GMR sensor has a high-sensitivity in the applied *B* range from -1 to 1 mT.

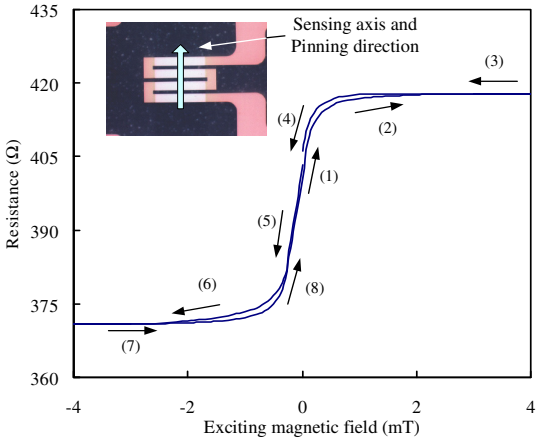

Fig. 14. DC characteristics of the GMR sensor

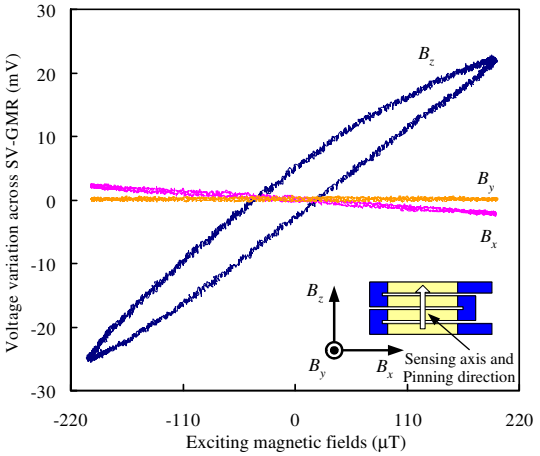

Fig. 15. Small signal AC characteristics of the GMR sensor at an exciting frequency of 100 kHz

Small signal AC characteristics of the GMR sensor in the *x*, *y* and *z* axes were tested with a *B* in the range of -200 to 200 μT; the detected *B* generated from eddy-current, for the purpose of PCB inspection, is smaller than ±200 μT. A DC bias current of 4 mA, the usual bias current used in the experiment, is applied to the GMR sensor. The small signal characteristics of the proposed GMR sensor are tested at a frequency of 100 kHz as shown in Fig. 15. From the characteristics it can be seen that the GMR sensor is most sensitive in the *z* (sensing) axis. The sensitivity of the proposed GMR sensor in the sensing axis is around 150 μV/μT.

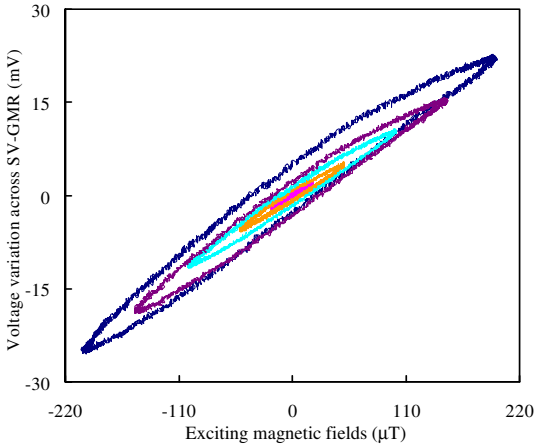

(a) Exciting frequency of 100 kHz.

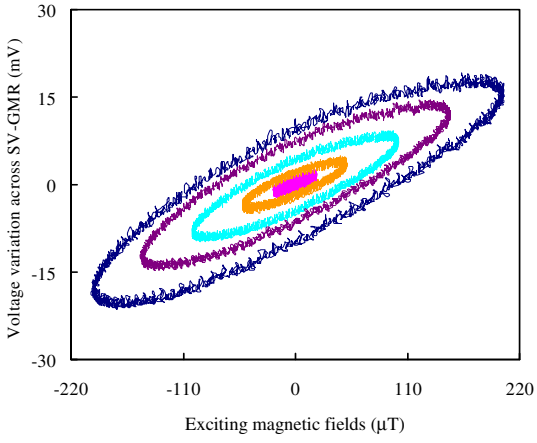

(b) Exciting frequency of 1 MHz.

Fig. 16. Effect of external magnetic flux amplitude on the GMR sensor output

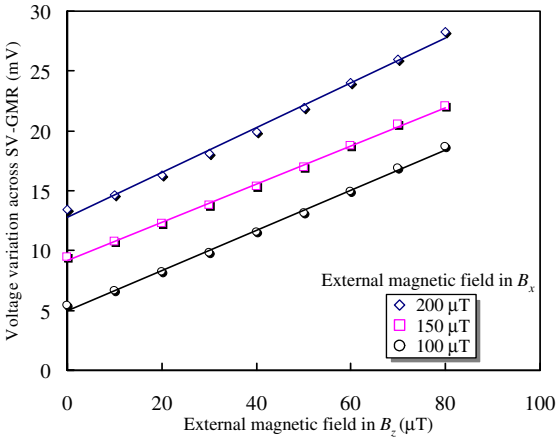

Fig. 17. Effect of an external magnetic flux density B_x on B_z and GMR sensor output

The sensitivity of the GMR sensor in the linear region is independent of the applied B amplitude as shown in Fig. 16. However, there is a marked increase in hysteresis with increasing B and frequency. Therefore, the GMR sensor used in the high-spatial ECT probe will be operated at magnetic flux densities lower than 20 μT; so that hysteresis effects will be at a minimum when the probe is used for defect detection. Planar meander coils normally generate a B in the x and y direction; therefore, experiments were done to observe the effect B_x has on the detection of B_z. Figure 17 shows the effect of constant external magnetic flux density B_x at the same frequency of magnetic flux density B_z and its effect on the GMR sensor output. It can be seen that the B_x results in a constant resistance variation, whereas resistance variation depends on the external magnetic flux density B_z. This shows that the constant magnetic flux densities in other axes have no effect on the detection of B_z.

2.3.2 Characteristics of the ECT Probe for PCB Inspection

Three types of defects on a PCB conductor are experimentally analyzed. 9 μm thick PCB conductors made from Cu coated with 0.05 μm Au were used as a PCB model with conductor disconnections and partial defects on the PCB track width as shown in Fig. 18. Conductor disconnections ranging from 50 to 500 μm were allocated on the PCB conductor as shown in Fig. 18 (a). Distance between the defects is 10 mm. For partial defects on PCB conductor track width, the conductor disconnection region was fixed at 100 μm as show in Fig. 18 (b). The conductor disconnection regions vary from 25 % of PCB track width to a total disconnection. For partial defects on PCB thickness, PCB conductors with thickness of 35 μm are used. Two chipping defects, as shown in Fig. 18 (c), were allocated on the model. The disconnection region is fixed at 100 μm as in the case of partial defect on PCB track width.

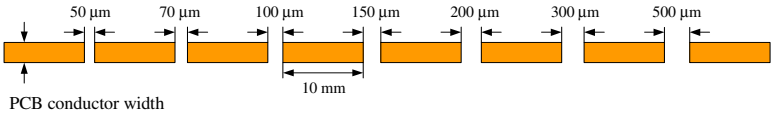

(a) Conductor disconnection model (top view).

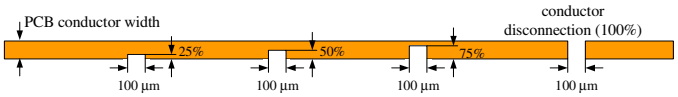

(b) Partial defect on PCB conductor track width (top view).

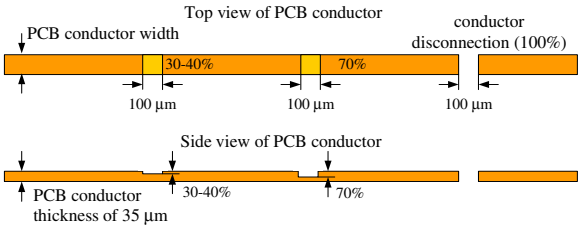

(c) Partial defect on PCB thickness.

Fig. 18. Model of defect on PCB conductor

The *B* generated by eddy-current flow at defect points on a PCB conductor can be detected by the ECT probe as shown in Fig. 19; the signal obtained from the ECT probe agrees with the aforementioned FEM analytical results. The signal has the same pattern and its amplitude depends on defect size; the phase of the ECT signal also varies at defect points. As shown in Figs. 20 and 21, although the ECT signal variations are very small, the utilization of the GMR sensor as a magnetic sensor provides the possibility of defect detection on a narrow, 50 µm wide, PCB conductor and a conductor disconnection length of 70 µm. The noise level is constant at around 0.7 µV. As shown in Fig. 21, signal variation depends on PCB conductor size and decreases almost linearly. Imperfections on a PCB conductor track width and thickness can also be inspected by the ECT probe. Figures 22 and 23 show the signal variations at partial defects on a PCB conductor track width and thickness, respectively. The signal variations at partial defects are lower than the signal variations at conductor disconnections. The signal variations at thickness defects are very small but large enough to identify the defect points.

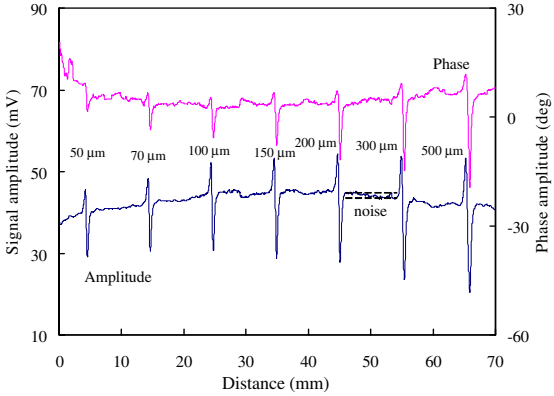

Fig. 19. ECT signal and its phase obtained from scanning over a 200 µm wide PCB conductor using the ECT probe

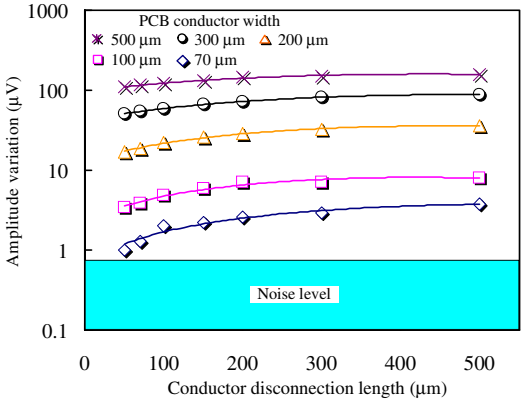

Fig. 20. Signal amplitude variation for different conductor disconnection lengths

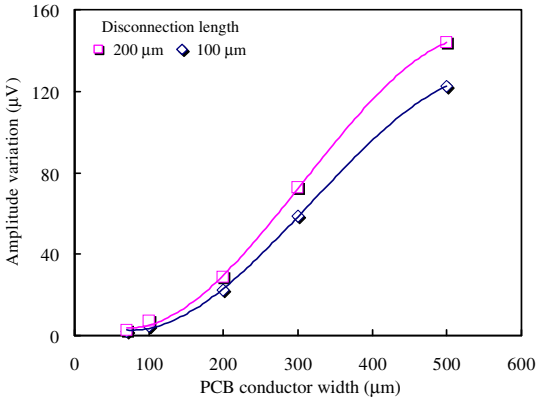

Fig. 21. Signal amplitude variation for different PCB conductor widths

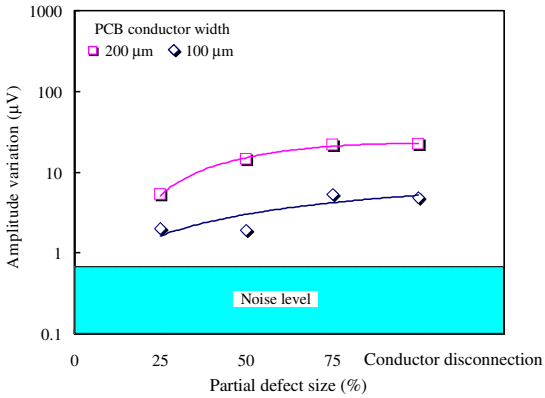

Fig. 22. Signal amplitude variation for partial defects on PCB conductor track widths

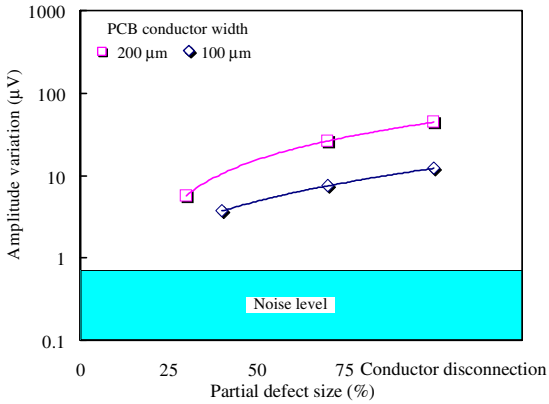

Fig. 23. Signal amplitude variation for partial defects on PCB conductor track thicknesses

The ECT signal waveforms in Fig. 24 obtained from the detection of a solder microbead with 125 µm radius at the frequency of 5 MHz and 10 MHz agree with the ECT signal waveforms obtained from FEM analysis. The determination of the microbead position is done by considering the peak of signal gradient. Figure 25 shows the maximum variation of the ECT signal versus the radius of the solder microbead, ranging from 125 to 300 µm. The maximum signal variation at an exciting frequency of 10 MHz decreases with the solder microbead radius and it is lower than the signal variation at exciting frequency of 5 MHz when the solder microbead radius is bigger than 200 µm. This is because the planar meander coil cannot generate a uniform B distribution. The experimental results also shows that signal variations at the solder microbead depend on the frequency of the exciting B and the solder microbead radius.

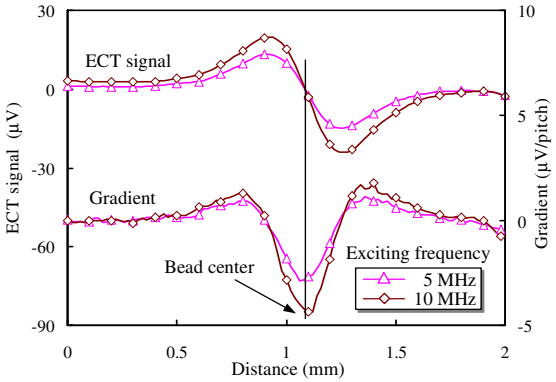

Fig. 24. ECT signal obtained from the detection of a solder microbead (PbSn) with 125 μm radius and its signal gradient

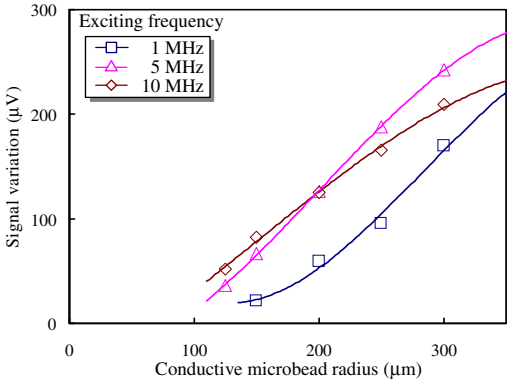

Fig. 25. Maximum signal variation vs. conductive microbead (PbSn) radius

2.3.3 PCB Inspection System

The PCB inspection system consists of two parts as shown in Fig. 26; the data acquisition process by the ECT technique and the image processing technique used to identify defect points on a PCB conductor. PCBs are scanned and the collected data is sent for identification of defects. The data acquisition apparatus consists of the ECT probe, a PCB position controller, exciting system, and measurement system, as shown in Fig. 27. The position controller is controlled by the computer for scanning regions on PCBs. High-frequency excitation at a frequency of 5 MHz is generated by a function generator and is fed to the power amplifier before feeding to the meander coil. The output signals from the ECT probe are very weak and comprise many unwanted signals; the harmonics and high-frequency noise. Therefore, the signal-to-noise ratio must be improved.

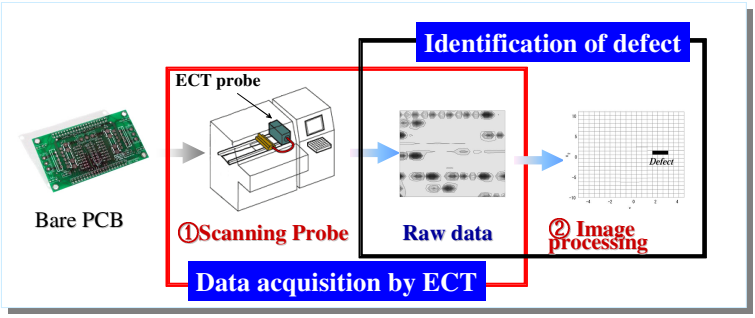

Fig. 26. PCB inspection system

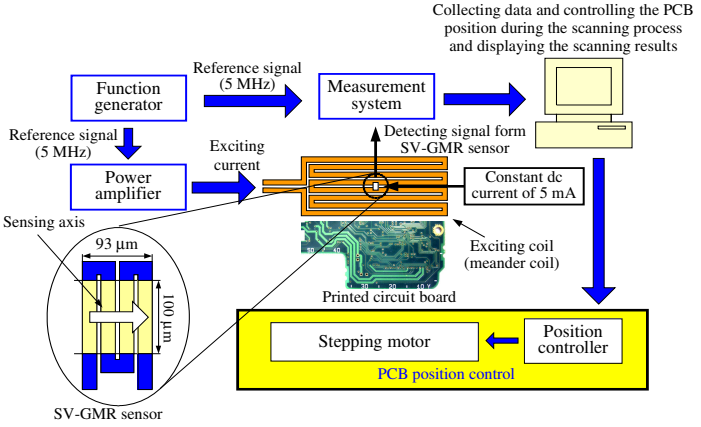

Fig. 27. Data acquisition system based on ECT technique

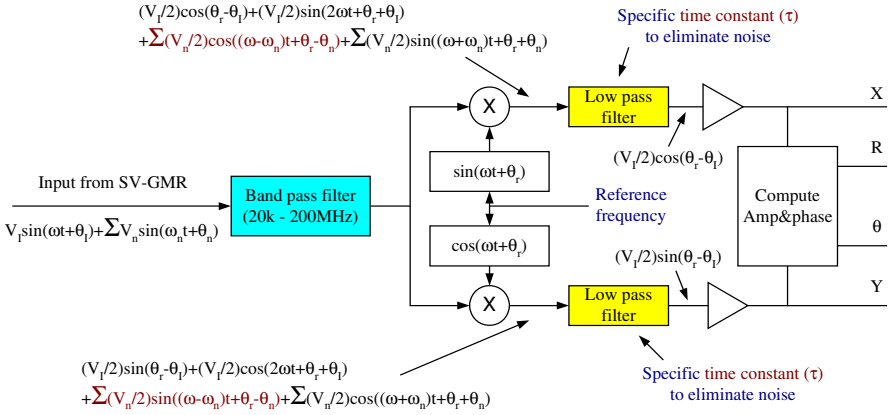

Fig. 28. Block diagram showing the basic principle of a lock-in amplifier

A lock-in amplifier based on phase-sensitive detection can be used to measure very small signals embedded in a lot of noise. This is because phase-sensitive detection can improve signal-to-noise ratio of noisy signals, which is usually higher than 60 dB [43]. A simple block diagram representing the basic principle of a lock-in amplifier is shown in Fig. 28. The input signal $v_{in}(t) = V_s \sin(\omega t + \theta_s) + \sum V_{noise} \sin(\omega_{noise} t + \theta_{noise})$, which consists of a signal and noise term, (where V_{noise}, ω_{noise}, and θ_{noise} are amplitude, frequency, and phase shift of the noise, respectively), is multiplied by the sine and cosine function at the fundamental frequency.

Therefore, the noisy signal can be obtained as following:

$$\begin{aligned} V_x/2 = {} & (V_s/2)\sin(\theta_r - \theta_s) + (V_s/2)\sin(2\omega t + \theta_r + \theta_s) \\ & + \sum (V_{noise}/2)\cos((\omega - \omega_{noise})t + \theta_r - \theta_{noise}) \\ & + \sum (V_{noise}/2)\sin((\omega + \omega_{noise})t + \theta_r + \theta_{noise}) . \end{aligned} \tag{4}$$

$$\begin{aligned} V_y/2 = {} & (V_s/2)\sin(\theta_r - \theta_s) + (V_s/2)\cos(2\omega t + \theta_r + \theta_s) \\ & + \sum (V_{noise}/2)\sin((\omega - \omega_{noise})t + \theta_r - \theta_{noise}) \\ & + \sum (V_{noise}/2)\cos((\omega + \omega_{noise})t + \theta_r + \theta_{noise}) . \end{aligned} \tag{5}$$

It can be seen from equations (4) and (5) that there are 3 components; DC, low-frequency, and high-frequency. Due to the relationship between time constant τ, and cut-off frequency f_c, the AC component can be rejected by the low pass filter resulting in only a DC component, by increasing the time constant τ. If the low-frequency component is very close to DC, time constant of the low pass filter needs to be increased in order to eliminate the low-frequency component. This means that the ECT probe have to wait until the lock-in amplifier acquires a steady state value before the ECT probe can be moved to measure the signal at the next position. This is a cause of scanning speed restriction if a lock-in amplifier is used to measure the ECT signal.

Fourier analysis can also be applied to measure low, noisy signals. By applying Fourier analysis on the measured signal, the signal amplitude at the required frequency can be extracted in a shorter time than by using a low pass filter. Amplitude of the signal at the fundamental frequency can be obtained within a few cycles of the measured frequency (5 MHz) [44]. Therefore, the PCB inspection with high-speed scanning can produce inspection results without or minimum distortion. A Fourier series is an expansion of a periodic function $f(t)$ in terms of an infinite sum of sines and cosines. The computation and study of Fourier's series is known as harmonic analysis and is extremely useful as a way to break up an arbitrary periodic function into a set of simple terms that can be plugged in, solved individually, and then recombined to obtain the solution to the original problem or an approximation to it to whatever accuracy is desired or practical.

A signal *f(t)* can be expressed by a Fourier's series in the form:

$$f(t) = a_0/2 + \sum_{n=1}^{\infty} \{a_n \cos(n\omega t) + b_n \sin(n\omega t)\}, \tag{6}$$

where n represents the rank of the harmonics (n = 1 corresponds to the fundamental component). The term $a_0/2$ represents the mean value or DC component of waveform and a_n and b_n are Fourier coefficients.

2.4 High-Density PCB Inspection

2.4.1 PCB Defect Inspection

As shown in Fig. 29, ten PCB conductors with different conductor widths, W, and gaps, G, was used as a model. Two PCB models were used:

1) 100 µm PCB conductor width, W, with 200 µm gap, G
2) 100 µm PCB conductor width, W, with 100 µm gap, G

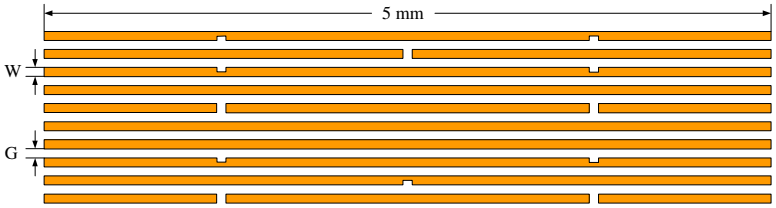

Fig. 29. Single layer PCB model used in an experiment

The PCB images and scanning results after image processing was applied, as shown in Fig. 30. The same defects were allocated on both the PCB models. The smallest conductor disconnection was only 20 µm. Furthermore, different kinds of partial defects were located on this model. The scanning results show that the ECT probe can inspect defects on a PCB conductor. From the inspection results of a bare PCB with a 100 µm track width, the defects on PCB conductor are not difficult to identify although the images are not clear. PCB conductor gap is one of the parameters that affect the signal variations. Signal variations at defect points decrease when the gap between PCB conductors is small and if the spatial resolution of the GMR sensor is not high enough. Hence, the spatial resolution needs to be increase for the inspection of high density PCBs that with less than 100 µm gap.

Distance between PCB conductors and sensing level is very important for inspection of the bottom-layer of double-layer PCBs. Figure 31 shows the inspection results obtained from scanning over a 100 µm wide PCB conductor. The GMR sensor can detect the *B* variation at defect points and provides variation of both signal amplitude and phase. The complex plane is convenient to represent the variation of both signal amplitude and phase at defect points as real and imaginary components. The results

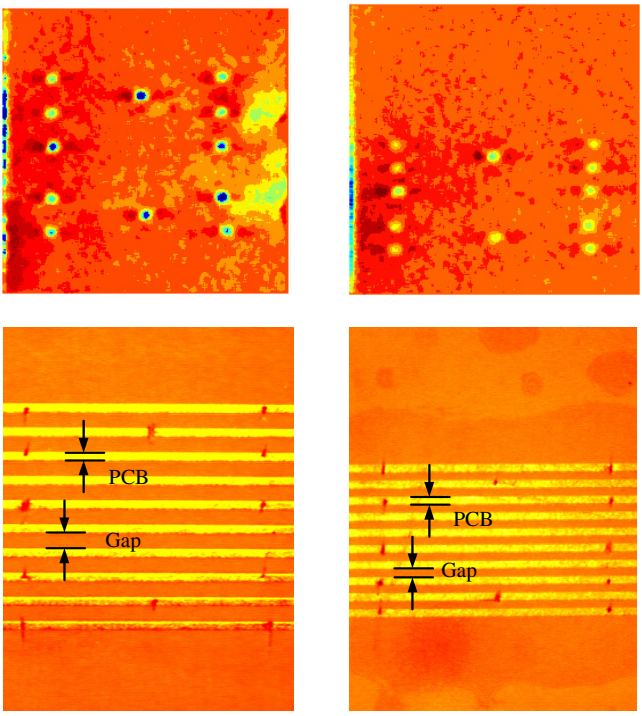

Fig. 30. Inspection results of the PCB model with 100 µm PCB conductor width (W) and gap (G) of 200 µm (left) and 100 µm (right)

show that the proposed ECT probe is able to inspect the defects on the PCB conductor with 235 µm lift-off height although the signal variations are very small. This means that the probe is capable of inspecting the defects at the bottom layer if the distance between PCB conductor and sensing level is less than 200 µm. Two models of high-density double-layer PCBs with a dimension of 5 mm × 5 mm as shown in Fig. 32 was used for experiments. Both models have a conductor width of 100 µm with 100 and 200 µm gaps between its conductors. The top layer has PCB conductors parallel to the *x* direction while the conductors are in the bottom layer. The disconnection and partial defects are also allocated on both the top and the bottom layer of the PCB model. 2-D images reconstructed from the ECT signals obtained from scanning over the top layer of the both PCB models in *x* and *y* directions are shown in Figs. 33 and Fig. 34. Numerical gradient technique is a simple image processing technique that is used to eliminate signal offset and to enhance the signal at the defect points. The 2-D images show that the proposed ECT probe is capable of inspecting the defect clearly although the defect points are also allocated on bottom layer of the test PCB. Moreover, not only conductor disconnections but also imperfections on PCB conductor can be detected.

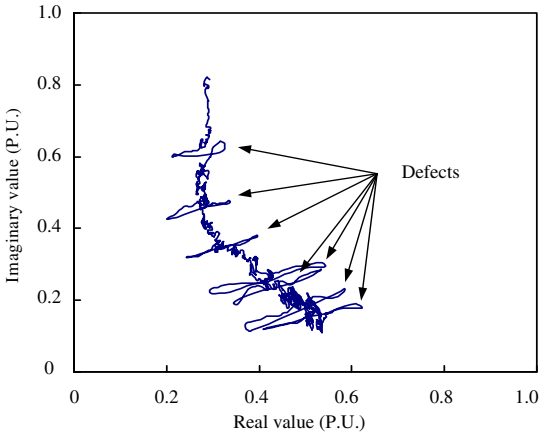

(a) Lift-off height = 185 µm

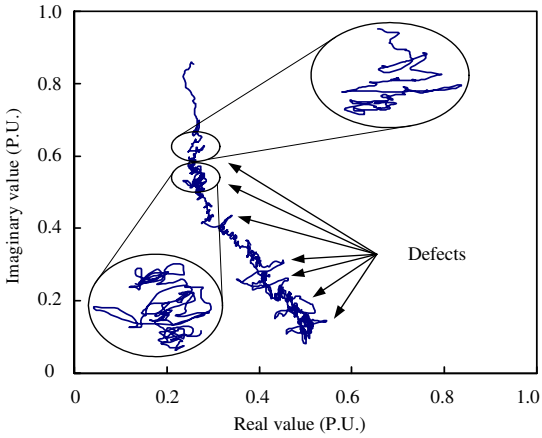

(b) Lift-off height = 235 µm

Fig. 31. Complex plane of ECT signal obtained from scanning over a 100 µm wide PCB conductor, at different distances from sensing level to the PCB conductor

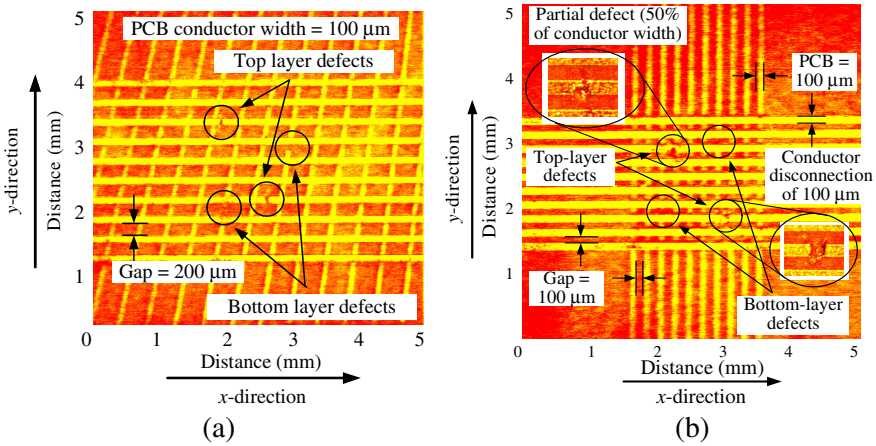

Fig. 32. Double layer PCB models. (a) 100 µm PCB conductor model with gap of 200 µm, and (b) 100 µm PCB conductor model with gap of 100 µm

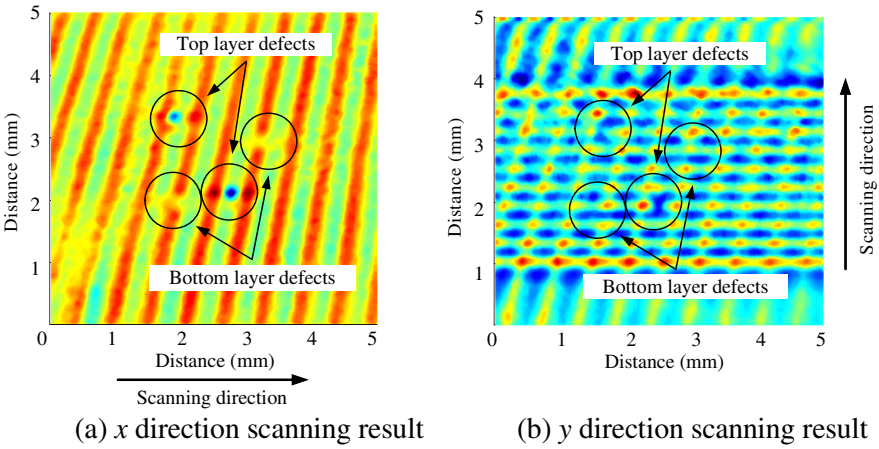

Fig. 33. PCB inspection results for a 100 µm conductor width with a gap of 200 µm

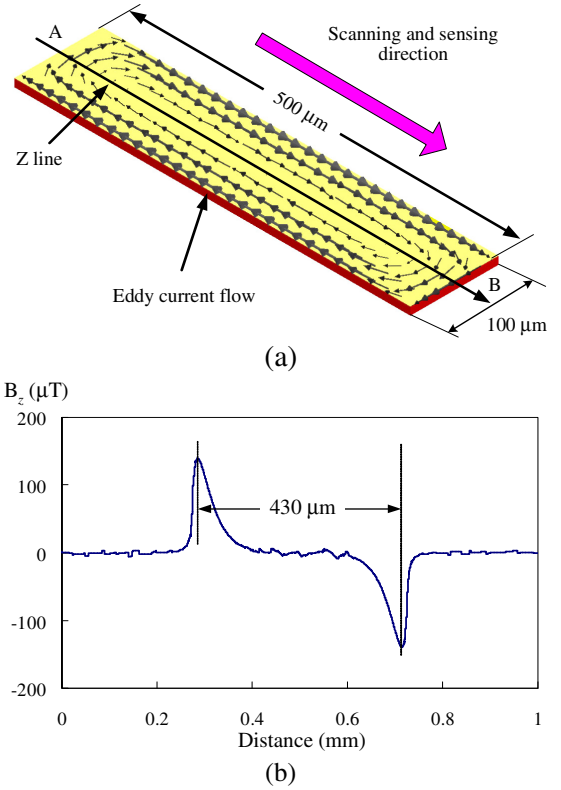

Fig. 34. Eddy-current flow (a) magnetic flux density over a PCB conductor in the sensing direction on the Z line from A to B; (b) when the probe scans along the PCB conductor

2.4.2 PCB Dimension and Alignment Inspection

Eddy-currents are usually distributed near the PCB conductor boundaries, as in Fig. 34 (a). Therefore, peak values of *B* in sensing direction occur near PCB conductor boundaries that are perpendicular to the scanning direction. These characteristics indicate that both length and width of the PCB conductor can specified by considering the peak values of *B* with measurement error less than 70 µm and 30 µm, for measurement of PCB conductor length and width, respectively. For precise measurement, exciting frequency should be higher than the frequency in simulation to generate eddy-currents flowing as close as possible to the PCB conductor boundary. Therefore, peak values of *B* in sensing axis will occur very close to PCB conductor boundary that is perpendicular to scanning direction. Absolute measurement errors, when the probe has been applied to measuring PCB conductor width and disconnection length, are shown in Fig. 35 (a) and (b) respectively. From these results, absolute measurement errors are lower than 100 µm for measurement of PCB conductor width. In case of conductor disconnection and PCB conductor length measurements, the absolute measurement errors are lower than 400 µm. However, it is not more than 200 µm when disconnection or gap between PCB conductors that are longer than 200 µm is measured.

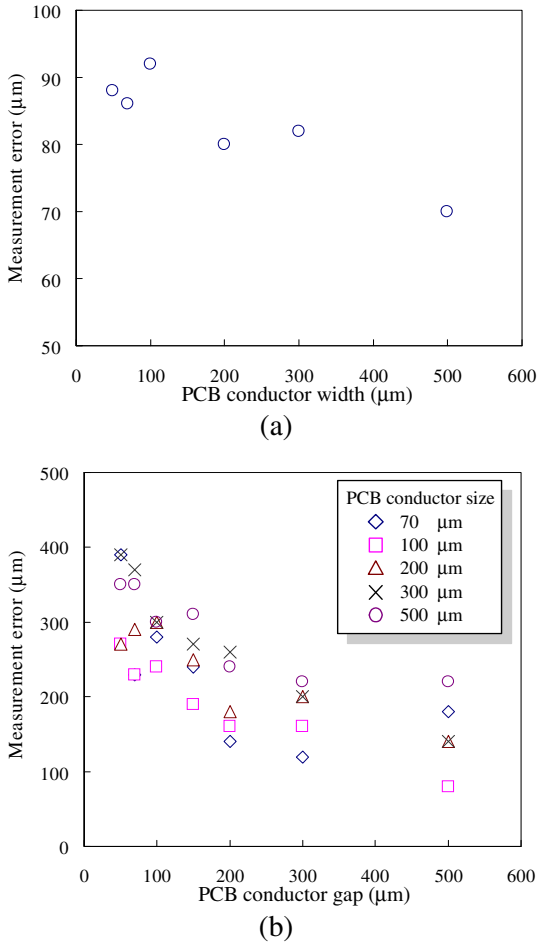

Fig. 35. Absolute measurement errors obtained when the ECT probe is used to measure PCB conductor width (a) and disconnection length (b)

High-density PCB models with 100 µm PCB conductor width were used as a model in the experiment and gap between the conductors is 100 µm, as shown in Fig. 36 (a). The high-density PCB model images and its reconstructed 2-D images from ECT signals without offset are shown in Fig. 36 (b). Conductor disconnection and partial defects were allocated on the conductor. Basic filtering techniques were applied to eliminate noise before the reconstruction of the 2-D image. From the reconstruction of the 2-D image, the defect points on the conductor were clearly identified. The PCB conductors are able to be identified by considering the peak of ECT signal as shown in the strip chart. Inspection of the larger gap model provided not only clearer details and easier identification of PCB conductor size but also gap between conductors (with error less than 100 µm) than the smaller gap model. In addition, the distance between

defect points, both the larger and smaller gap model, is also able to be specified accurately with an error less than 200 µm. However, more effective image processing techniques should be applied to improve the information [45, 46].

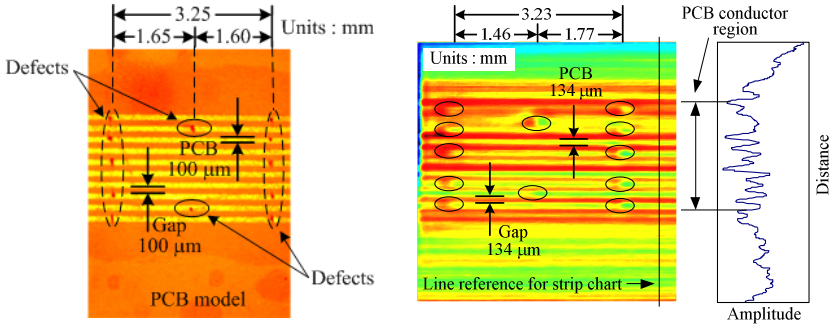

Fig. 36. High-density PCB images of a 100 µm wide PCB conductor; (a) inspection results (b) with gaps of 100 µm. The strip charts obtained from the line reference show the high signal variation occurring at the PCB conductor region.

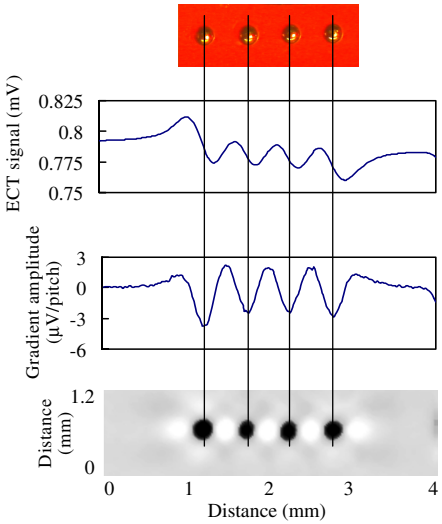

Fig. 37. Identification of the solder microbeads by the application of numerical gradient to the ECT signals

2.4.3 Ball Grid Array Detection

The numerical gradient technique is applied to ECT signals obtained from the detection of solder microbeads [47, 48]. The results show that the numerical gradient is able to enhance the signal at the microbead as shown in Fig. 37. As a result, the microbead position is easily identified by considering the peak of the signal gradient.

In addition, the pitches of the conductive microbead are also measured by considering the peak of the signal gradient. The solder microbead array model with 250 µm diameter and 410 – 460 µm microbead pitches and its detection results are shown in Figs. 38 (a) and (b) respectively. The proposed ECT probe scans over the solder microbead with areas of 4 mm × 4 mm. Form the detection results, the solder microbeads are clearly recognized and the pitches of the conductive microbead are also accurately specified with errors within 50 µm.

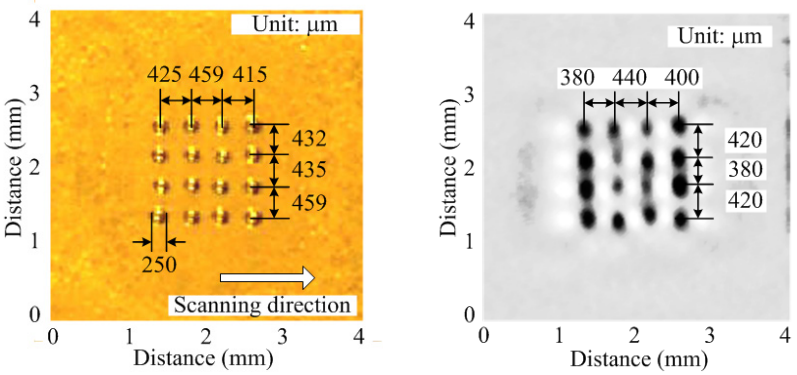

Fig. 38. Solder microbead array model (a) and its detection results (b)

3 Conclusions

The design and development of an ECT probe for high-density PCB inspection was reported in this section. The ECT probe consists of a magnetic sensor and a planar meander coil functioning as an exciting coil. A GMR was chosen as the magnetic sensor because it provides the advantages of high-spatial resolution due to small dimensions, high sensitivity to low magnetic fields over a broad range of frequencies. Moreover, it is inexpensive and is able to operate at room temperature. Behavior of eddy-current flow and magnetic flux distribution was studied using FEM and the results confirmed that the proposed ECT probe can be applied to high-density PCB inspection.

The GMR sensor was characterized in order to determine its capability of magnetic field detection and sensitivity; these results were used to develop a high performance ECT probe. Characterization of the probe with GMR sensor showed that measurement could be performed with high signal-to-noise ratio. Furthermore, the probe with GMR sensor is capable of defect detection on PCB conductor with width of 70 µm and thickness of 9.05 µm. Three kinds of defect were tested in the experiment. The first was conductor disconnection, the second was partial defect on PCB track width, and the third was partial defect on PCB thickness. The results show that the inspection results can be performed by the proposed ECT probe. Inspection of high-density

single and double layer PCB models were demonstrated. Inspection of the PCB model with conductor width and gap of 100 μm was performed by the proposed ECT probe. In case of double layer PCB inspection, the probe is capable of inspecting the defects at the bottom layer if the distance between PCB conductor and sensing level is not over 200 μm. Moreover, dimension and alignment of PCB conductor can also be examined. Consideration of the peak of magnetic flux density that usually occurs at boundary of PCB conductor is useful for investigation of PCB dimensions and alignment. The inspection results showed that the proposed ECT probe is able to examine PCB conductor dimensions and alignment with an error less than 200 μm. Furthermore, the ECT probe was also successfully utilized to detect the position of 125 μm radius solder microbeads on a BGA.

Acknowledgment. The authors would like to thank Professor Masayoshi Iwahara (Retired) from the Institute of Nature and Environmental Technology, Kanazawa University, for his help in this research. Thank you to Professor Hiroyuki Wakiwaka from Shinshu University for the advice and support about GMR sensors. The authors gratefully acknowledge research support from the Ministry of Education, Culture, Sports, Science and Technology (MEXT) and the Japan Society for Promotion of Science (JSPS).

References

[1] Smith, C.H., Schneider, R.W.: Low-Field Magnetic Sensing with GMR Sensors Part 1: The Theory of Solid-State Sensing. Sensors 16, 76–83 (1999)
[2] Schneider, R.W., Smith, C.H.: Low Magnetic Field Sensing with GMR Sensors Part 2: GMR Sensors and Their Applications. Sensors 16, 84–91 (1999)
[3] Wakiwaka, H.: Characteristics of Giant Magnetoresistance Sensor and Their Applications. Journal of the Magnetics Society of Japan 28, 825–833 (2004)
[4] Schewe, H., Schelter, W.: Industrial applications of magnetoresistive sensors. Sensors and Actuators A 59, 165–167 (1997)
[5] Tumanski, S.: Thin Film Magnetoresistive Sensors. Institute of Physics, London (2001)
[6] Tsymbal, E.Y., Pettifor, D.G.: Perspectives of Giant Magnetoresistance. In: Ehrenreich, H., Spaepen, F. (eds.) Solid State Physics, pp. 113–237. Academic Press, California (2001)
[7] Daughton, J.M.: GMR applications. Journal of Magnetism and Magnetic Materials 192, 334–342 (1999)
[8] Lenz, J., Edelstein, A.S.: Magnetic Sensors and Their Applications. IEEE Sensors Journal 6, 631–649 (2006)
[9] Dieny, B.: Giant magnetoresistance in spin-valve multilayers. Journal of Magnetism and Magnetic Materials 136, 335–359 (1994)
[10] Dogaru, T., Smith, S.T.: Giant Magnetoresistive-Based Eddy Current Sensor. IEEE Transactions on Magnetics 37, 3836–3838 (2001)
[11] Childress, J.R., Fontana Jr, R.E.: Magnetic recording read head sensor technology. Comptes Rendus Physique 6, 997–1012 (2005)
[12] Gooneratne, C.P., Liang, C., Giouroudi, I., Kosel, J.: An integrated micro-chip for rapid detection of magnetic particles. Journal of Applied Physics 111, 07B327 (2012)

[13] Gooneratne, C.P., Liang, C., Giouroudi, I., Kosel, J.: A giant magnetoresistance ring-sensor based microsystem for magnetic bead manipulation and detection. Journal of Applied Physics 109, 07E517 (2011)
[14] Smith, C.H., Schneider, R.W., Dogaru, T., Smith, S.T.: Eddy-current testing system with GMR magnetic sensor arrays. Review of Progress in Quantitative Nondestructive Evaluation 2323, 406–413 (2003)
[15] Reig, C., Cubells-Beltrán, M.D., Muñoz, D.R.: Magnetic Field Sensors Based on Giant Magnetoresistance (GMR) Technology: Applications in Electrical Current Sensing. Sensors 9, 7919–7942 (2009)
[16] Freitas, P.P., Ferreira, H.A., Graham, D.L., Clarke, L.A., Amaral, M.D., Martins, V., Fonseca, L., Cabral, J.M.S.: Magnetoresistive DNA Chips. In: Johnson, M. (ed.) Magnetoelectronics, pp. 331–396. Academic, New York (2004)
[17] Miller, M.M., Sheehan, P.E., Edelstein, R.L., Tamanaha, C.R., Zhong, L., Bounnak, S., Whitman, L.J., Colton, R.J.: A DNA array sensor utilizing magnetic microbeads and magnetoelectronic detection. Journal of Magnetism and Magnetic Materials 225, 138–144 (2001)
[18] Gaster, R.S., Xu, L., Han, S.J., Wilson, R.J., Hall, D.A., Osterfeld, S.J., Yu, H., Wang, S.X.: Quantification of protein interactions and solution transport using high-density GMR sensor arrays. Nature Nanotechnology 6, 314–320 (2011)
[19] Schwartz, W.H.: Vision Systems for PC Board Inspection. Assembly Engineering 29, 18–21 (1986)
[20] Barnard, S.T.: Automatic Visual Inspection of Printed Circuit Boards. In: Advanced Systems for Manufacturing: Conference on Production Research and Technology, pp. 423–429 (1985)
[21] Mukai, S.: PCB Continuous Line System Proceeds from Manufacturing to Inpsection. Journal of Electronic Engineering 29, 34–39 (1992)
[22] Foster, J.W., Griffin, P.M., Messimer, S.L., Villalobos, J.R.: Automated Visual Inspection: A Tutorial. Computers in Industrial Engineering 18, 493–504 (1990)
[23] Goodall, A.J.E., Lo, E.K.: A Review of Inspection Techniques Applicable to PCB Manufacturing and Assembly particularly with respect to SMT. Advanced Manufacturing Engineering 3 (1991)
[24] Hroundas, G.: Importance of Electrical Inspection for the Printed Circuit Board. In: Proceedings of the Circuit Expo West, pp. 53–60 (1986)
[25] Jacob, G.: Advances in Board Inspection. Evaluation Engineering, 126–133 (1992)
[26] García-Martin, J., Gómez-Gil, J., Vázquez-Sánchez, E.: Non-Destructive Techniques Based on Eddy Current Testing. Sensors 11, 2525–2565 (2011)
[27] Le Bihan, Y., Pávó, Marchand, C.: Characteristics of small cracks in eddy current testing. The European Physics Journal Applied Phyics 43, 231–237 (2008)
[28] Hellier, C.J.: Handbook of Nondestructive Evaluation. McGraw-Hill (2001)
[29] Shull, P.J.: Nondestructive Evaluation Theory, Technique, and Applications. Marcel Dekker Inc. (2002)
[30] Burkhardt, G.L., Fisher, J.L.: Nondestructive Testing of Aging Aircraft. Southwest Research Institute Technology Today (2001)
[31] Dogaru, T., Smith, S.T., Smith, C.H., Schneider, R.W.: Eddy Current Inspection for Deep Crack Detection Around Fastener Holes in Airplane Multi-Layered Structures. In: 3rd Pan American Conference for Nondestructive Testing, Rio de Janeiro, Brazil, (2003)
[32] Dogaru, T., Smith, S.T.: Novel Eddy Current Probes for Detection of Deep Cracks Around Fastener Holes. In: Fifth Joint NASA/DOD/FAA Aging Aircraft Conference, Orlando, USA (2001)

[33] Ko, R.T., Petricola, D.L., Berens, A.P., Rambo, M.: A Study of Index Step Sizes for Varing Coil Diameters and Their Effects on Throughput and Probability of Detection (POD) for Improved Automated Eddy Current Inspections on Areospece Engine-Components. In: 16th World Conference on Nondestructive Testing, Montreal, Canada (2004)

[34] Stanic, D., Elsing, B.: Eddy Current Inspection of Cladding Material on VVER440 Reactor Pressure Vessels. In: 16th World Conference on Nondestructive Testing, Montreal, Canada (2004)

[35] Muzhitsky, V.F., Karabchevsky, V.A., Karpov, S.V.: Ten Years of Experience of Stress-Corrosion and Other Pipelines' Surface Flaws Testing by Means of Eddy Current Technique. In: 16th World Conference on Nondestructive Testing, Montreal, Canada (2004)

[36] Crowther, P.: Non Destructive Evaluation of Coatings for Land Based Gas Turbines Using a Multi-Frequency Eddy Current Technique. In: 16th World Conference on Nondestructive Testing, Montreal, Canada (2004)

[37] Tian, H., Yamada, S., Iwahara, M., Toyama, H., Miya, K.: Eddy-Current Model and Detection in a Thick Stainless Steel Plate. Transaction on Magnetics Society of Japan 5, 39–42 (2005)

[38] Rao, B.P.C., Jayakumar, T., Kalyanasundaram, P., Raj, B.: An Insight into Design and Development of Eddy Current Sensors for Non-Destructive Evaluation of Materials. In: Proceedings of the National Workshop on Sensors, Kalpakkam, India (2000)

[39] Dogaru, T., Smith, C.H., Smith, S.T.: New Directions in Eddy Current Sensing. Sensors Magazine 18 (2001)

[40] Mulligan, C., Lee, C., Danon, Y.: Characterization of Magnetron Sputtered Coating by Pulsed Eddy Current Techniques. Review of Progress in Quantitative Nondestructive Evaluation 24, 1721–1728 (2005)

[41] Nakamura, K., Yamada, S., Iwahara, M.: Inspection of Printed Circuit board Using Multi-ECT Probe with Solenoid Pickup Coils. Journal of the Magnetics Society of Japan 26, 555–558 (2002)

[42] Yamada, S., Nakamura, K., Iwahara, M., Taniguchi, T., Wakiwaka, H.: Application of ECT Technique fro Inspection of Bare PCB. IEEE Transactions on Magnetics 39, 3325–3327 (2003)

[43] Standford Research Systems, User's Manual: Model SR844 RF Lock-In Amplifier, Standford Research Systems. Rev. 2.5, USA, 2-3–2-18 (1997)

[44] Chomsuwan, K., Yamada, S., Iwahara, M.: Bare PCB Inspection System with SV_GMR Sensor Eddy-Current Testing Probe. IEEE Sensors Journal 7, 890–896 (2007)

[45] Taniguchi, T., Kacprzak, D., Yamada, S., Iwahara, M.: Wavelet-Based Processing of ECT Images for Inspection of Printed Circuit Boards. IEEE Transactions on Magnetics 37, 2790–2793 (2001)

[46] Kacprzak, D., Taniguchi, T., Nakamura, K., Yamada, S., Iwahara, M.: Superposition of Signal Components During Inspection of Printed Circuit Boards by an Eddy Current Testing Probe With a Solenoid Pick-Up Coil. IEEE Transactions on Magnetics 37, 2794–2796 (2001)

[47] Yamada, S., Chomsuwan, K., Hagino, T., Tian, H., Minamide, K., Iwahara, M.: Conductive Microbead Array Detection by High-Frequency Eddy-Current Testing technique with SV-GMR Sensor. IEEE Transaction on Magnetics 41, 3622–3624 (2005)

[48] Somsak, T., Chomsuwan, K., Yamada, S., Iwahara, M.: Conductive Microbead Array Detection Based on Eddy-Current Testing Using SV-GMR Sensor and Helmholtz Coil Exciter. IEEE Transactions on Magnetics 42, 3572–3574 (2006)